Biochemistry and Biophysics Reports 9 (2017) 193–202

Contents lists available at ScienceDirect

Biochemistry and Biophysics Reports

journal homepage: www.elsevier.com/locate/bbrep

Development of a subunit vaccine for prevention of *Clostridium difficile* associated diseases: Biophysical characterization of toxoids A and B

Alexey Gribenko, Elena Severina, Maninder K. Sidhu, Kathrin U. Jansen, Bruce A. Green, Yury V. Matsuka*

Pfizer Vaccine Research and Development, 401 N. Middletown Road, Pearl River, NY 10965, USA

ARTICLE INFO

Keywords:
C. difficile
Subunit vaccine
Toxins/toxoids A and B
Biophysical characterization

ABSTRACT

Inactivation of bacterial toxins for use in human vaccines traditionally is achieved by treatment with formaldehyde. In contrast, the bivalent experimental vaccine for the prevention of *C. difficile* infections (CDI) that is currently being evaluated in clinical trials was produced using a different strategy. *C. difficile* toxins A and B were inactivated using site-directed mutagenesis and treatment with 1-ethyl-3-[3-dimethylaminopropyl]carbodiimide hydrochloride/*N*-hydroxysulfosuccinimide (EDC/NHS). In the present work we investigate the effect of genetic and chemical modifications on the structure of inactivated toxins (toxoids) A and B. The far-UV circular dichroism (CD) spectra of wild type toxins, mutated toxins, and EDC/NHS-inactivated toxoids reveal that the secondary structure of all proteins is very similar. The near-UV CD spectra show that aromatic residues of all proteins are in a unique asymmetric environment, indicative of well-defined tertiary structure. These results along with the fluorescence emission maxima of 335 nm observed for all proteins suggest that the tertiary structure of toxoids A and B is preserved as well. Analytical ultracentrifugation data demonstrate that all proteins are predominantly monomeric with small fractions of higher molecular weight oligomeric species present in toxoids A and B. Differential scanning calorimetry data reveal that genetic mutations induce thermal destabilization of protein structures. Subsequent treatment with EDC/NHS results either in a minimal (1 °C) increase of apparent thermostability (toxoid B) or no change at all (toxoid A). Therefore, our two-step inactivation strategy is an effective approach for the preparation of non-toxic proteins maintaining native-like structure and conformation.

1. Introduction

Clostridium difficile is a spore-forming, Gram-positive pathogenic bacterium that causes gastrointestinal infections, often following antibiotic treatment, and is a key cause of nosocomial illness worldwide [1]. *C. difficile* toxins A and B are the major virulence factors responsible for the induction of pseudomembranous colitis (PMC) and antibiotic-associated diarrhea in humans [1,2]. The action of *C. difficile* toxins A and B include binding to the surface of the epithelium, endocytosis-dependent entrance to the cell, passage through an acidic environment of the early endosome, and release into the cytosol. Inside the cell both toxin A and toxin B catalyze O-glucosylation of specific threonine residues within the Rho family of GTPases involved in the regulation of actin polymerization and fiber assembly. These modifications disrupt the integrity of the cytoskeleton and subsequently lead to rounding of cells and apoptosis [1,3].

Despite recent progress in the understanding of the molecular mechanisms of clostridial pathogenesis, current options for treatment of *C. difficile* infections (CDI) are limited and often ineffective [4]. Antibiotic-based therapies routinely consist of treatment with metronidazole and vancomycin, which contribute to the disruption of the intestinal microbiota and often result in relapses of CDI upon completion of antibiotic course [5]. Therefore, alternative therapeutic strategies including immune-based approaches become increasingly important for successful management of CDI [6]. Several lines of evidence indicate that immune-based therapies and active vaccination could be effectively utilized for treatment and prevention of CDI. Firstly, it was demonstrated that an antibody response to *C. difficile* toxins correlates

Abbreviations: TcdA, wild type toxin A; TM TcdA, D285A/D287A/C700A toxin A triple mutant; TxdA, EDC/NHS-treated D285A/D287A/C700A toxoid A triple mutant; TcdB, wild type toxin B; TM TcdB, D286A/D288A/C698A toxin B triple mutant; PM TcdB, D286A/D288A/C698A/E970K/E976K toxin B penta mutant; TxdB, EDC/NHS-treated D286A/D288A/C698A toxoid B triple mutant; EDC, 1-ethyl-3-[3–dimethylaminopropyl]carbodiimide hydrochloride; NHS, *N*-hydroxysulfosuccinimide; CD, circular dichroism spectroscopy; DSC, differential scanning calorimetry; ANS, 1-anilinonaphtalene-8-sulfonic acid; PBS, Phosphate buffered saline

* Corresponding author.
E-mail address: yury.matsuka@pfizer.com (Y.V. Matsuka).

http://dx.doi.org/10.1016/j.bbrep.2016.12.015
Received 6 July 2016; Received in revised form 7 December 2016; Accepted 20 December 2016
Available online 05 January 2017

with resistance to infection and with protection against recurrent infections [7,8]. Secondly, the efficacy of active vaccination using inactivated toxins (toxoids) was shown in hamster studies [9–11] and the feasibility of successful vaccination demonstrated in humans [12]. It is commonly accepted that efficacious vaccination should result in production of high levels IgG antibodies capable of neutralizing cytotoxic activity of *C. difficile* toxins A and B [13]. Such a requirement emphasizes the importance of understanding structural features of toxins as well as the necessity to preserve these features (*i.e.* critical epitopes) upon inactivation of toxins for subsequent use in the vaccine.

C. difficile toxins A and B are large multidomain proteins that exhibit multiple common structural and functional features. Toxin A consists of 2710 residues (308.0 kDa) and toxin B of 2366 residues (269.6 kDa) [3]. Both toxins A and B are composed of distinct domains each of which is responsible for a specific biological activity [3,14]. The glucosyltransferase domain is situated in the N-terminal portion of toxin A and B and ultimately responsible for their known cytotoxic activity. The conserved DXD motif, which is involved in manganese coordination, is a distinguishing feature of this domain [15]. Adjacent to the N-terminal glucosyltransferase domain is the cysteine protease domain. The cysteine protease domain is characterized by a catalytic triad composed of aspartate, histidine, and cysteine residues (DHC) [16]. The protease domain is essential for auto-cleavage and release of the catalytic glucosyltransferase domain into the cytosol. A short hydrophobic region located in the middle part of both the toxin A and B polypeptide chains may contribute to membrane translocation of the catalytic domain [17]. The C- terminus of the clostridial glucosylating toxins is known as the cell wall binding domain, and consists of 20 or 30 residue repeats. These repeats ensure an initial interaction of the toxin with the surface of the mammalian cell by binding to the carbohydrate moieties of unidentified glycoprotein receptor(s) [18].

Recently we reported a novel approach for endogenous expression of *C. difficile* toxins A and B utilizing a plasmid-based system and a non-sporulating strain of *C. difficile* as a host [19]. Toxins A and B expressed in this system contained three point mutations of aspartic acid and cysteine residues (D285A/D287A/C700A in toxin A and D286A/D288A/C698A in toxin B) that drastically reduced but did not completely eliminate the cytotoxic activity of the proteins [19]. Furthermore, additional mutations of two conserved glutamic acids (E970K and E976K) participating in pore formation and translocation of toxin B [20] further reduced, but still did not abolish, cytotoxicity of the protein [19].

To abrogate residual cytotoxic activity, genetically altered toxins (triple mutant toxin A and triple mutant toxin B) were subjected to chemical inactivation using 1-ethyl-3-[3-dimethylaminopropyl]carbodiimide hydrochloride and *N*-hydroxysulfosuccinimide (EDC/NHS treatment) [21]. EDC/NHS-treatment of triple mutant preparations of toxoid A and B eliminated detectable cytotoxic activity [21]. The degree of EDC/NHS-induced modification, as well as the exact positions of modified amino acid residues within both antigens, was characterized in detail using tryptic mapping and mass spectral analysis. These EDC/NHS-treated toxoids A and B lacking detectable cytotoxic activity elicited toxin neutralizing antibodies when used to immunize mice and hamsters [21]. Currently, the bivalent toxoid A- and toxoid B-based experimental vaccine is undergoing a Phase 2 (NCT02561195) clinical trial sponsored by Pfizer (clinicaltrials.gov).

In the present study we report the results of a comparative biophysical characterization of the wild type toxins (TcdA, TcdB), toxins with three amino acid substitutions (TM TcdA, TM TcdB), and EDC/NHS-inactivated toxoids (TxdA, TxdB). We investigated whether amino acid substitutions and EDC/NHS treatment inactivation steps were accompanied by changes in toxins A and B protein structure and/or conformation. To evaluate the possible effect of genetic and chemical modifications on higher order (*i.e.* secondary, tertiary) protein structure, we employed circular dichroism (CD) spectroscopy, fluorescence spectroscopy, analytical ultracentrifugation (AUC), and differential scanning calorimetry (DSC). The data revealed that inactivated toxoids A and B (TxdA and TxdB) maintain secondary/tertiary structure and conformation similar to that of the functionally active wild type toxins. These results are discussed with regard to the current practices of toxin inactivation and in the context of an ongoing clinical trial with the *C. difficile* toxoid A and B vaccine.

2. Materials and methods

2.1. Proteins

Recombinant TcdA, TcdB, TM TcdA, and TM TcdB were produced in an asporogenic strain of *C. difficile* [19]. All wild type toxins and genetic mutants were purified from the soluble fraction of cell lysate as previously described [21]. The EDC/NHS treatment of the triple mutants and preparation of TxdA and TxdB was reported by Vidunas et al. [21].

2.2. SDS-PAGE analysis

SDS-PAGE was performed with the Invitrogen Novex Mini-Cell electrophoresis system (Invitrogen) using precast 10% Tris-Gly gels. The samples were prepared by adding 4X Nu PAGE LDS Sample buffer (Invitrogen) followed by heating at 90 °C for 5 min either without reducing agent (non-reducing condition) or in the presence of 10% (vol/vol) 2-mercaptoethanol (Bio-Rad) (reducing condition). All SDS-polyacrylamide gels in this study were stained with Coomassie Blue ("SimplyBlue SafeStain") (Invitrogen).

2.3. Sample preparations for biophysical measurements

All toxin and toxoid preparations were aliquoted and stored frozen at −20 °C. To prepare protein samples for biophysical measurement, frozen stocks were thawed and centrifuged at 14,000 rpm for 10 min at 4 °C (Eppendorf Centrifuge 5417R). Supernatants were extensively dialyzed at 4 °C against PBS, pH 7.4. Protein concentrations were determined spectrophotometrically using a Cary 300 Bio UV–vis spectrophotometer (Varian). The extinction coefficients at 280 nm were calculated from amino acid composition using the ProtParam tool (http://expasy.org/tools/protparam.hl). The extinction coefficients were found to be 1.275 $(mg/ml)^{-1}$ cm^{-1} and 1.067 $(mg/ml)^{-1}$ cm^{-1} for the wild type toxin/toxoid A and the wild type toxin/toxoid B, respectively. Correction for light scattering was taken into account as described by Winder and Gent [22]. Partial specific molar volumes of the proteins, buffer density and buffer viscosity under experimental conditions used were calculated using Sednterp software (http://www.jphilo.mailway.com/download.h).

2.4. Circular dichroism (CD) spectroscopy

CD experiments were done on a Jasco J-810 spectropolarimeter (Jasco Inc) in rectangular quartz cells (Starna Cells) with path lengths of 1 mm (far-UV CD) or 1 cm (near-UV CD). All CD spectra were recorded at 20 °C with scan rates of 50 nm/min, response time of 1 s and bandwidth of 3 nm. Temperature was controlled using Peltier-type PTC-423S temperature controller (Jasco Inc). Far-UV CD spectra were recorded from 200 to 260 nm. Protein concentration during the far-UV CD experiments was maintained at ~0.2 mg/ml. Near-UV CD spectra were recorded from 250 to 320 nm, with sample concentrations ranging from 0.2 to 1.0 mg/ml. Precise protein concentrations for calculating mean residue ellipticity or molar ellipticity were determined spectrophotometrically after each CD scan, as described above. CD data were processed by subtracting the buffer spectrum (blank) from the sample spectrum and smoothed by the nearest neighbor averaging of 21 points. Mean residue ellipticity in units of mdeg cm^2dmol^{-1} was calculated as

$$\Theta_{MRE} = \frac{\Theta_{\exp} \cdot (M_w/N)}{10 \cdot c \cdot l} \quad (1)$$

where Θ_{MRE} is calculated mean residue ellipticity, Θ_{exp} is experimentally measured ellipticity in mdeg, M_w is protein molecular weight, N is the number of amino acid residues, c is protein concentration in mg/ml, l is the optical path length in cm. Molar ellipticity in units of mdeg cm^2 mol^{-1} was calculated as

$$\Theta_{molar} = \frac{\Theta_{\exp}}{C \cdot l} \quad (2)$$

where Θ_{molar} is calculated molar ellipticity, Θ_{exp} is experimentally measured ellipticity in mdeg, C is protein concentration in mol/L, l is optical path length in cm.

2.5. Intrinsic and extrinsic fluorescence spectroscopy

Intrinsic fluorescence emission spectra were recorded between 300 and 400 nm in 1 cm quartz cuvette on a Jasco FP-6500 fluorescence spectrometer (Jasco) at the medium sensitivity setting using an excitation wavelength of 280 nm, with excitation and emission band paths set to 3 nm and 5 nm, respectively. Intrinsic fluorescence emission spectra were recorded at 20 °C. Temperature was controlled using Peltier type ETC-273T temperature controller (Jasco). Protein concentration was maintained at 0.02 mg/ml in all experiments. Samples were allowed to equilibrate for 15 min at the experimental temperature before the measurements were taken. Fluorescence intensity was recorded every 0.1 nm. Five accumulations of each spectrum were collected and averaged. Protein spectra were corrected for the buffer contribution by subtracting the fluorescence spectrum of the buffer recorded under identical conditions and further smoothed by the nearest neighbor averaging of 21 points.

Temperature-induced unfolding experiments were carried out on an SLM Aminco Bowman Series 2 luminescence spectrometer (Thermo) in a 1 cm quartz cell at the protein concentration of 0.02 mg/ml in all experiments. Temperature was controlled using a circulating water bath (PolyScience, model 1157) programmed to raise the temperature at ~1 °C/minute. The temperature was monitored with an Omega DP81 digital thermometer and an external HYP-1 thermocouple probe (Omega) inserted into a parallel dummy cell filled with water. Upon sample equilibration at the starting point (21 °C), temperature of the water bath was set to 85 °C and the changes in the ratio of the fluorescence intensity at 350 nm versus 320 nm upon excitation at 280 nm were recorded every 0.5 s using custom-written software. The fluorescence ratio parameters were instantly plotted in real time as a function of the actual temperature reading from the external probe inserted into the dummy cell. Excitation and emission band paths were set to 4 nm. The data were smoothed using SigmaPlot software, version 11.1.

2.6. Analytical ultracentrifugation (AUC)

Analytical ultracentrifugation experiments were performed on a Beckman XL-I analytical ultracentrifuge (Beckman). Sedimentation velocity runs were done at 40,000 rpm, 20 °C using analytical cells equipped with quartz windows and sector-shaped 2-channel centerpieces. Boundary movement was monitored using UV-absorbance of the sedimenting solutes at 280 nm. Protein concentrations were adjusted to give A_{280} of ~0.3–0.7 absorbance units. Data were fit to the continuous C(s) distribution model using SedFit software [23] developed by Peter Schuck (www.analyticalultracentrifugation.com). Apparent sedimentation coefficient distributions, C(s), were calculated as described in the SedFit manual. Identical frictional ratio (f/f_O) was assumed for all of the sedimenting species in a given cell during the fit. Resulting apparent sedimentation coefficients (s) were then converted into standard sedimentation coefficients, $S_{(20\ °C,w)}$ using Sednterp (i.e., into sedimentation coefficients that would be observed in pure water at 20 °C) to eliminate effects of solvent density, viscosity and protein concentration on the observed hydrodynamic behavior of the molecules. Standard frictional ratios, $f/f_{O(20\ °C,w)}$, were calculated from the frictional coefficients of the proteins under standard conditions, $f_{(20\ °C,w)}$, and frictional coefficients of ideal spheres of the same molecular weight, $f_{O(20\ °C,w)}$, respectively calculated as

$$f_{(20^oC,w)} = \frac{M \cdot (1 - \overline{V}\rho)}{N \cdot S_{(20^0C,w)}} \quad (3)$$

$$f_{0,(20^oC,w)} = 6\pi\eta\left(\frac{3V_{anh}}{4\pi}\right)^{1/3} \quad (4)$$

where M is a known molecular weight of the protein under study, $\overline{V}$ is partial specific molar volume (0.735 cm^3/g and 0.734 cm^3/g for toxins A and B, respectively), ρ is water density at 20 °C (0.9982g/cm^3), N is Avogadro's number (6×10^{23}), η is water viscosity at 20 °C (0.01002 Poise), V_{anh} is the anhydrous volume of the protein molecule. An assumption was made that introduced amino acid substitutions or EDC treatment had no appreciable effect on the partial specific molar volumes of the proteins. At least two experiments were done in all cases with average values and standard deviations of the resulting parameters given in Table 1.

2.7. Differential scanning calorimetry (DSC)

Differential scanning calorimetry experiments were performed on either a VP-capillary DSC (TcdA, TM TcdA, TxdA) or VP-DSC (TcdB, TM TcdB, TxdB) differential scanning microcalorimeters (GE Healthcare). Capillary DCS was used for all toxin/toxoid A species as these proteins exhibited a tendency to precipitate during unfolding in a microcalorimeter equipped with a conventional cell. DSC runs with 20–25 identical scans were typically programmed and started the night before each set of the experiments to ensure baseline equilibration. Baseline stability was verified the next morning by comparing several consecutive buffer-buffer scans recorded overnight. Protein samples were loaded between successive scans without stopping the DSC run. Reference cells of the calorimeters were filled with dialysate. Protein samples at concentrations of 0.3–1.0 mg/ml (5–27 μM, depending on the particular experiment) were typically scanned from 5 °C to 75 °C at the scan rates of 60 °C/h (TcdA, TM TcdA, TxdA) or 90 °C/h (TcdB, TM TcdB, PM TcdB, TxdB), with pre-scan thermostat of 5–15 min and filtering period of 8–16 s. Data were analyzed using Origin 7.0 software provided by the DSC manufacturer. Heat capacity profiles of the individual proteins were corrected by subtracting buffer-buffer scans from the protein data and normalized by protein concentration.

3. Results

3.1. Homogeneity and electrophoretic mobility

The effect of amino acid substitutions and EDC/NHS treatment on the structural characteristics of *C. difficile* toxins and toxoids was investigated by comparing each toxin to its cognate toxoids, e.g., TcdA to TM TcdA, and TxdA and TcdB to TM TcdB, and TxdB. These proteins were expressed, isolated, and chemically modified as described elsewhere [19,21]. Each of toxin/toxoid A and toxin/toxoid B species utilized in this study displayed a single NH_2-terminal sequence starting at SLISKEELIKLAYSI and SLVNRKQLEKMANVR, respectively. The homogeneity of all proteins was evaluated by SDS-PAGE under non-reducing and reducing conditions (Fig. 1A and B). The TcdA, TM TcdA, TcdB, and TM TcdB predominantly migrated as single bands with relative mobilities slightly higher than their expected monomeric molecular masses. Minor low mobility bands visible in TcdA, TM TcdA, TcdB, and TM TcdB preparations at non-reducing

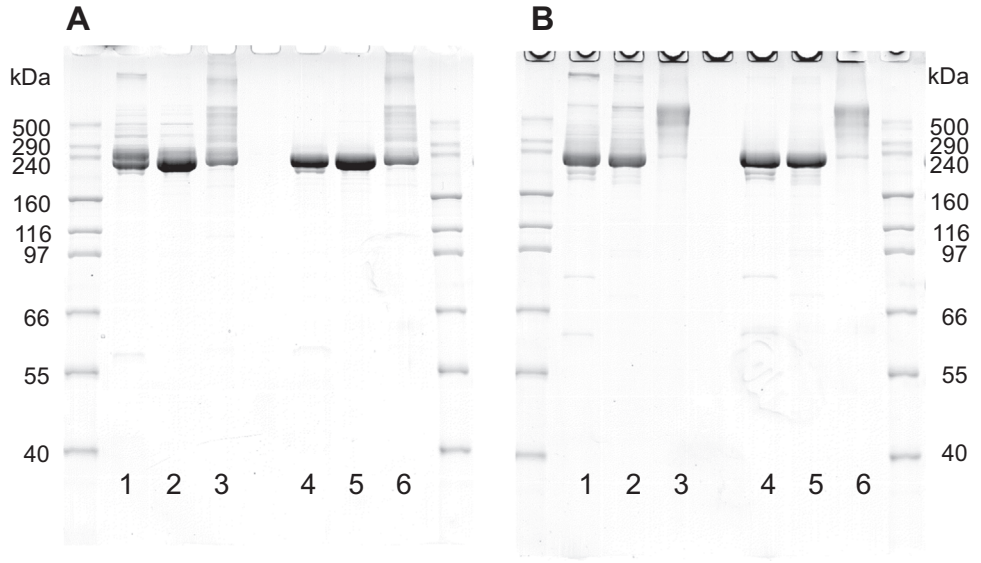

Fig. 1. SDS-PAGE analysis of toxins/toxoids A (panel A) and B (panel B) at non-reducing and reducing conditions. Panel A: TcdA (lane 1- non reducing, lane 4 - reducing), TM TcdA (lane 2- non reducing, lane 5-reducing), and TxdA (lane 3-non reducing, lane 6-reducing). Panel B: TcdB (lane 1-non reducing, lane 4- reducing), TM TcdB (lane 2-non reducing, lane 5 - reducing), and TxdB (lane 3 - non reducing, lane 6 - reducing). The outer lanes on both gels contain molecular mass standards as indicated.

conditions (Fig. 1A and B, lanes 1, 2) and disappearance of these bands upon reduction (Fig. 1A and B, lanes 4, 5) indicate that a small fraction of the molecules are linked to each other via disulfide bond(s) to form higher molecular mass species. EDC/NHS treatment of TM TcdA and TM TcdB resulted in the appearance of a broad range of low mobility bands (Fig. 1A and B, lanes 3). Both TxdA and TxdB samples exhibited identical SDS-PAGE patterns under non-reducing (Fig. 1A and B lanes 3) and reducing (Fig. 1A and B lanes 6) conditions suggesting that their electrophoretic properties are defined exclusively by EDC/NHS modification(s).

3.2. Secondary and tertiary structure

We used circular dichroism (CD) and fluorescence spectroscopy to analyze and compare higher-level structural organization of the wild type toxins, their corresponding genetic mutants, and EDC/NHS-treated toxoids. All proteins show well-defined far-UV CD spectra (Fig. 2A and B), indicating that the proteins possess defined secondary structure (far-UV CD spectra of the unfolded TcdA and TcdB in 6 M Gdm-HCl are shown for comparison). The shape of the far-UV CD spectra and presence of characteristic negative bands at 208 nm and 222 nm suggests that the secondary structures of all proteins are dominated by α-helices (Fig. 2A and B). Furthermore, neither amino acid substitutions nor EDC/NHS treatment had noticeable effects on the far-UV CD spectra, indicating that secondary structures of TM TcdA, TM TcdB, TxdA, and TxdB are largely the same as that of the corresponding wild type toxins (TcdA and TcdB).

The high intensity of the near-UV CD spectra (Fig. 3A and B) show that at physiological conditions aromatic residues of all proteins are in the unique asymmetric environment, indicative of well-defined tertiary structure (near-UV CD spectra of the unfolded wild type toxins A and B in 6 M Gdm-HCl are shown for comparison). Near-UV CD spectra of TcdA, TM TcdA, and TxdA are identical, suggesting that their tertiary structures are identical as well. Near-UV CD spectrum of TM TcdB is very similar to the TcdB, while TxdB noticeably deviates from the other two proteins. Nevertheless, the near-UV CD spectral intensity of TxdB is significantly higher than that of the unfolded protein (Fig. 3B, dotted line). Based on these considerations it is apparent that the TxdB largely retains its tertiary structure.

Intrinsic fluorescence emission is a convenient tool for structural analysis of both *C. difficile* toxin A and toxin B since toxin A contains 25 tryptophan residues while toxin B contains 16. These intrinsic fluorophores are spread throughout the protein sequences and, correspondingly, report on global structural environment. Intrinsic fluorescence spectra of the proteins upon excitation at 280 nm are shown in Fig. 4A and B. Emission maxima of both TcdA and TcdB are 335 nm under native conditions (PBS, pH 7.4, t=20 °C), indicating that tryptophan residues are mainly in a non-polar environment, such as hydrophobic cores of the folded proteins [24]. This observation is consistent with earlier reported fluorescence maxima of 334 nm [25] and in agreement with our CD data, showing that all of the proteins under study retain compact folded structure. In the presence of 6 M Gdm-HCl the fluorescence emission maximum shifts to ~350 nm (Fig. 4A and B, dotted lines), consistent with the tryptophan residues now being exposed to the aqueous environment due to protein unfolding. Emission maxima of TM TcdA, TxdA, TM TcdB, and TxdB are identical to the corresponding wild type toxins (TcdA and TcdB), indicating that neither amino acid substitutions nor EDC/NHS treatment had noticeable effects on the folding state of the proteins.

3.3. Hydrodynamic properties

Hydrodynamic properties of TcdA, TM TcdA, TxdA, TcdB, TM TcdB, and TxdB were analyzed using analytical ultracentrifugation. Sedimentation velocity runs were performed as described in Materials and Methods. Data are presented in Fig. 5 and Table 1. Sharp peaks in the calculated sedimentation coefficient distributions (C(s)) indicate the presence of the well-defined discrete species (Fig. 5). Apparent molecular weights (calculated with the assumption that the frictional ratio (f/f_O) is the same throughout the distribution) suggest that all proteins are predominantly monomeric (Table 1). Small fractions of higher molecular weight species were evident in the case of TxdA and TxdB.

Sedimentation coefficients of the major peaks are the same (within experimental error) between the wild type toxins and corresponding mutated or EDC/NHS-treated proteins. Given that sedimentation coefficients depend on the molecular weights and shapes of the molecules, we can conclude that EDC/NHS treatment has not affected the overall shape of the molecules. Frictional ratios, which are directly related to the hydrodynamic shape of the molecules are also the same (Table 1). To summarize, the analytical ultracentrifugation results show that *C. difficile* wild type toxins, as well as corresponding

Table 1
Hydrodynamic parameters of *C. difficile* toxins/toxoids A and B.

Protein	$\bar{V}$, cm^3/g	S, svedberg	$M_{w,\ app}$, kDa	$S^0_{20\ ^\circ C,w}$, svedberg	$(f/f_0)^0_{20\ ^\circ C,w}$
TcdA	0.735	9.8 ± 0.1	280 ± 10	10.2 ± 0.2	1.58 ± 0.02
TM TcdA	0.735	9.8 ± 0.2	279 ± 7	10.2 ± 0.2	1.58 ± 0.02
TxdA	0.735	9.8 ± 0.2	276 ± 22	10.2 ± 0.2	1.58 ± 0.03
TcdB	0.734	9.9 ± 0.2	255 ± 25	10.3 ± 0.2	1.45 ± 0.02
TM TcdB	0.734	9.6 ± 0.2	246 ± 3	9.9 ± 0.2	1.49 ± 0.04
TxdB	0.734	9.7 ± 0.1	243 ± 9	10.1 ± 0.1	1.47 ± 0.01

Partial specific molar volumes ($\bar{V}$) were calculated from amino acid composition using SednTerp, sedimentation coefficients (S) were obtained from fitting sedimentation velocity data to the continuous C(s) distribution model with the assumption of the identical frictional ratio for all of the sedimenting species, $M_{w,\ app}$ – apparent molecular weights calculated for the major peak in the C(s) distribution using best-fit frictional ratios (expected molecular weights are 308 kDa for the wild type toxin A and 270 kDa for the wild type toxin B), $S^0_{20^oC,w}$ standard sedimentation coefficients corrected for buffer density, viscosity and protein concentration; $(f/f_0)^0_{20^oC,w}$– standard frictional ratios calculated from standard sedimentation coefficients and known protein molecular weights, as described in "Materials and Methods".

genetically and EDC/NHS modified proteins are elongated, predominantly monomeric molecules. Oligomeric species present in TxdA and TxdB are formed as a result of EDC/NHS treatment.

3.4. Thermostability

Thermostability of TcdA, TcdB, TM TcdA, TxdA, TM TcdB, and TxdB was initially compared using fluorescence spectroscopy (Fig. 6A and B). The thermal unfolding curve of TcdA shows a single transition, with the apparent transition midpoint of ~49 °C. Given the large size and multidomain organization of the protein, it is likely that the unfolding curve represents multiple overlapping transitions. Unfolding of TM TcdA shows two well-defined transitions, with the apparent midpoint of the first ~8 °C lower than that of the wild type toxin A. This decrease in the unfolding temperature indicates that D285A, D287A and C700A mutations destabilize the glucosyltransferase and/or cysteine protease domains of TcdA. Two transitions are also evident in the unfolding curve of the TxdA, although the midpoints are higher than observed in the case of the triple mutant.

Unfolding data collected for the TcdB, TM TcdB, and TxdB using

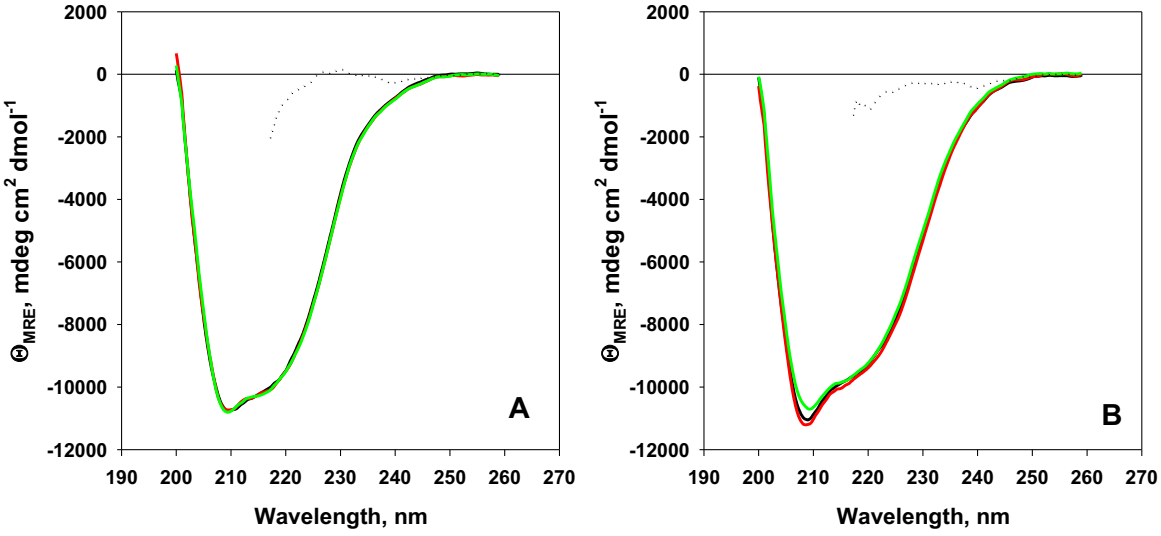

Fig. 2. Far-UV circular dichroism spectra of toxins/toxoids A (panel A) and B (panel B). Panel A: black solid line – TcdA, red solid line – TM TcdA, green solid line – TxdA, black dotted line – TcdA in 6 M Gdm-HCl; Panel B: black solid line – TcdB, red line – TM TcdB, green solid line – TxdB, black dotted line – TcdB in 6 M Gdm-HCl.

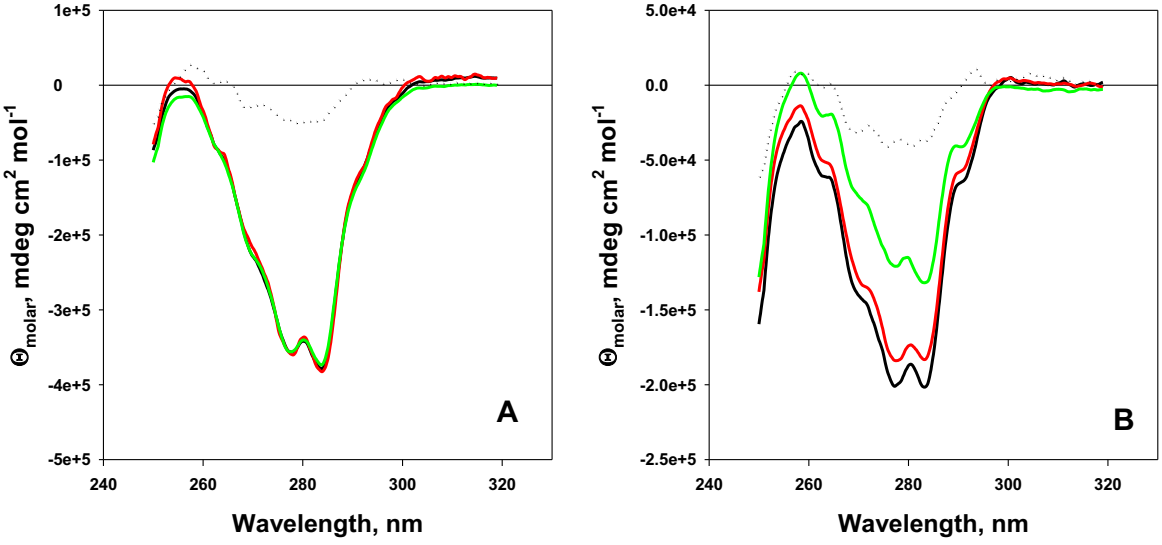

Fig. 3. Near-UV circular dichroism spectra of toxins/toxoids A (panel A) and B (panel B). Panel A: black solid line – TcdA, red solid line – TM TcdA, green solid line – TxdA, black dotted line – TcdA in 6 M Gdm-HCl; Panel B: black solid line – TcdB, red line – TM TcdB, green solid line – TxdB, black dotted line – TcdB in 6 M Gdm-HCl.

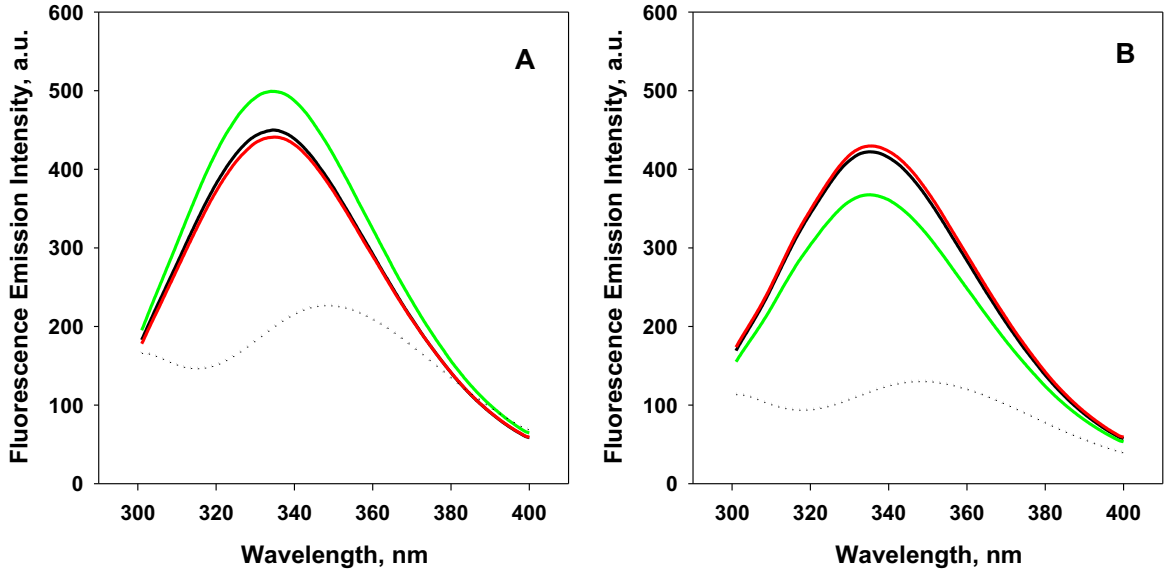

Fig. 4. Intrinsic fluorescence emission spectra of toxins/toxoids A (panel A) and B (panel B). Panel A: black solid line – TcdA, red solid line – TM TcdA, green solid line – TxdA, black dotted line – TcdA in 6 M Gdm-HCl; Panel B: black solid line – TcdB, red line – TM TcdB, green solid line – TxdB, black dotted line – TcdB in 6 M Gdm-HCl.

this approach are more complex and harder to interpret. The change in the fluorescence intensity ratio is biphasic: the ratio initially decreases upon increase in temperature to 40–42 °C and then increases upon further temperature increase. We cannot estimate the transition midpoints, as we do not know how close the first unfolding phase is to completion before the second phase begins. The overall shape of the TcdB unfolding curve is clearly different from that of the TM TcdB. This change in shape is not very informative for the reasons described above. We can say, however, that EDC/NHS treatment stabilized at least part of the TxdB molecule similarly to TxdA, as the second phase of the unfolding transition represented by the increase in the fluorescence ratio is clearly shifted to the higher temperatures. To gain better understanding of the unfolding process of *C. difficile* wild type toxins, as well as of their genetically and chemically modified counterparts, we employed DSC.

DSC results are presented in Fig. 7 and Table 2. As is expected for such large multidomain proteins, the thermograms contain multiple overlapping peaks. Unfolding of all evaluated proteins is irreversible, making rigorous thermodynamic analysis impossible. Complexity of the unfolding profiles and irreversibility of unfolding suggest that quantitative interpretation of the DSC results would not be meaningful. The transition midpoint temperatures reported in Table 2 do not represent true thermodynamic unfolding temperatures for the reasons described above, but rather are cumulative averages of multiple overlapping unfolding transitions. We used these numbers to estimate relative apparent thermostability of the proteins, therefore, only qualitative analysis of the DSC results is described. Similar to the fluorescence unfolding curves which contain two unfolding transitions, DSC thermograms recorded for TcdA, TM TcdA, and TxdA contain two excess heat capacity peaks. In agreement with the fluorescence data, DSC results suggest that D285A, D287A and C700A amino acid substitutions led to destabilization of the glucosyltransferase and/or

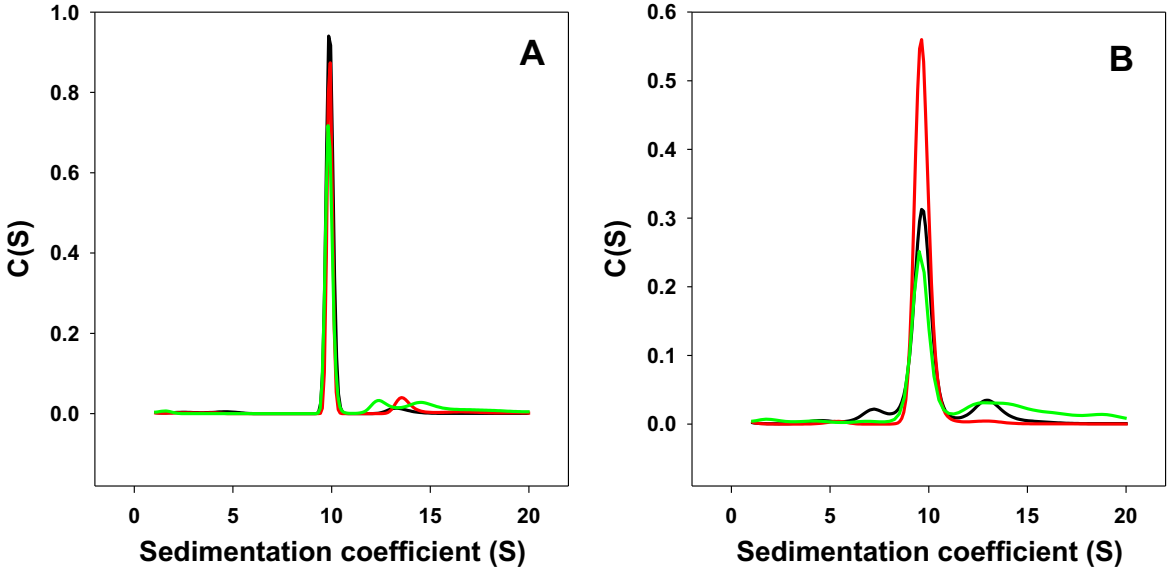

Fig. 5. Overlay of the C(s) distributions calculated from the sedimentation velocity experiments for toxins/toxoids A (panel A) and B (panel B). Panel A: black solid line – TcdA, red solid line – TM TcdA, green solid line – TxdA, black dotted line – TcdA in 6 M Gdm-HCl; Panel B: black solid line – TcdB, red line – TM TcdB, green solid line – TxdB, black dotted line – TcdB in 6 M Gdm-HCl. Sedimentation coefficient ranges between 1 and 20 only are shown for clarity, although actual ranges used in the fitting of the EDC-treated toxoid data had to be increased up to 100 S due to the presence of small fractions (< 1% of total absorbance) of higher molecular weight species.

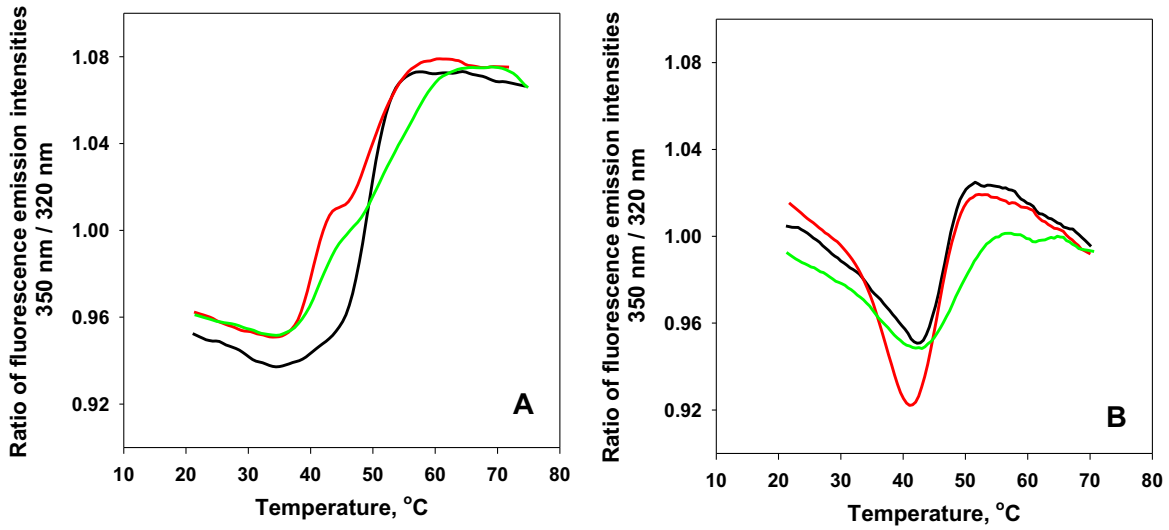

Fig. 6. Temperature-induced unfolding of toxins/toxoids A (panel A) and B (panel B) monitored via recording fluorescence emission ratio at 350 nm over 320 nm as a function of temperature. Panel A: black solid line – TcdA, red solid line – TM TcdA, green solid line – TxdA, black dotted line – TcdA in 6 M Gdm-HCl; Panel B: black solid line – TcdB, red line – TM TcdB, green solid line – TxdB, black dotted line – TcdB in 6 M Gdm-HCl. Colors and lines are the same as in Figs. 1–4. Data were smoothed using the smoothing option in SigmaPlot 11.0.

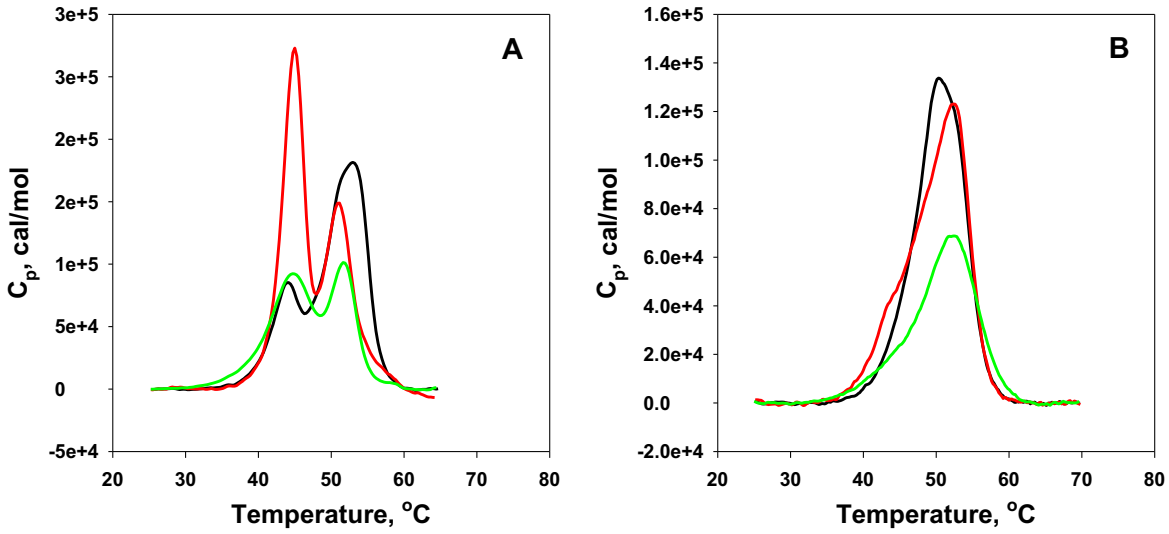

Fig. 7. Temperature-induced unfolding of toxins/toxoids A (panel A) and B (panel B) monitored by DSC. Panel A: black solid line – TcdA, red solid line – TM TcdA, green solid line – TxdA, black dotted line – TcdA in 6 M Gdm-HCl; Panel B: black solid line – TcdB, red line – TM TcdB, green solid line – TxdB, black dotted line – TcdB in 6 M Gdm-HCl. Heat capacity profiles were normalized by protein concentration for proper comparison.

Table 2
Apparent transition midpoints (T_m) of *C. difficile* toxins/toxoids A and B.

Toxin/toxoid A	T_{m1}, °C	T_{m2}, °C	Toxin/toxoid B	T_{m1}, °C	T_{m2}, °C
TcdA	44	53	TcdB	ND[a]	50
TM TcdA	45	51	TM TcdB	ND[a]	52
TxdA	45	52	TxdB	ND[a]	52

Apparent transition midpoints were estimated from peak maxima on the DSC thermograms.

[a] ND – Not detected.

protease domains (Fig. 7A). The area of the higher temperature transition (which is proportional to the amount of heat absorbed upon unfolding) and high temperature transition maximum are lower in the case of TM TcdA. On the contrary, the area of the low temperature peak is significantly increased, indicating that these amino acid substitutions shifted unfolding of the corresponding domain(s) towards lower temperature. In the case of TxdA, the total area of both excess heat capacity peaks is much smaller than observed for either TcdA or TM TcdA, which suggests that conformational transition of TxdA upon unfolding is not as dramatic as in the case of the two parent proteins. Comparison of the apparent unfolding temperatures (Table 2) shows that the change in the apparent thermostability of TxdA is minimal, suggesting that EDC/NHS inactivation introduced minimal changes in the native structure of the protein.

The DSC thermogram of TcdB contains only a single peak (Fig. 7B), which is clearly asymmetric, again indicating that the protein unfolds via multiple overlapping transitions. Introduction of the D286A, D288A and C698A substitutions increases asymmetry of the excess heat capacity peak of TM TcdB. A noticeable shoulder is appearing now at a lower temperature (~43 °C), while the peak maximum actually shifts to higher temperature (~52 °C), suggesting slight separation of at least two unfolding events that were represented by the single overlapping peak in TcdB. These DSC results are consistent with fluores-

cence detected denaturation data and also explain the observed change in the shape of the fluorescence unfolding curves of TM TcdB (Fig. 6B). Comparison of the DSC and fluorescence data suggests that the initial phase of the fluorescence unfolding curve corresponds to the unfolding of the glucosyltransferase and/or cysteine protease domain(s) (since they are less thermostable), with amino acid substitutions destabilizing the respective domain(s) and shifting this initial phase towards an even lower temperature. This shift results in greater separation of the unfolding transitions and a deeper trough observed in the fluorescence unfolding curves. Similarly to the TxdA, EDC/NHS treatment of TM TcdB results in a lower amount of heat absorbed upon unfolding of TxdB. Furthermore, unfolding of TxdB appears to be more cooperative than TM TcdB (a single asymmetric peak is observed, Fig. 7B), suggesting that EDC/NHS treatment may have resulted in increased interdomain interactions. Finally, EDC/NHS treatment had no noticeable effect on apparent thermostability of TxdB, as can be judged by the DSC results (Table 2).

3.5. Conformational plasticity

Acidification in early endosomes is thought to trigger a conformational change in the *C. difficile* toxins, which is necessary for membrane insertion and glucosyltransferase domain delivery into the cell cytoplasm [3,14,26]. pH-induced changes resulting in exposure of hydrophobic surfaces on the toxins are viewed as a critical prerequisite for insertion into the membrane. To evaluate if site directed mutagenesis or EDC/NHS treatment would have any effect on the capacity of the TxdA and TxdB to undergo conformational rearrangements in response to changes in pH, we employed extrinsic fluorescence spectroscopy and fluorescent dye 1-anilinonaphtalene-8-sulfonic acid (ANS). Binding of ANS probe to the hydrophobic surfaces results in increased fluorescence, which can be used to monitor conformational changes taking place in proteins. Changes in the ANS fluorescence intensity at different pH values in the presence of the TcdA, TM TcdA, TxdA, TcdB, TM TcdB, and TxdB are illustrated in Fig. 8A and B. A decrease in pH upon addition of the concentrated acidic buffer results in dramatic increase in the ANS fluorescence, regardless of whether wild type toxins, mutants or EDC/NHS modified proteins are present. Adding the same amount of phosphate and citrate at neutral pH had no effect on ANS fluorescence (data not shown), indicating that it is the pH drop, rather than change in the ionic strength or in the buffer composition that triggers conformational change in the proteins. These results clearly demonstrate that amino acid substitutions and EDC/NHS treatment had no effect on the structural plasticity of the vaccine candidates and that TxdA and TxdB closely resemble the wild type toxins.

4. Discussion

Traditionally, inactivation of bacterial toxins for use in human vaccines is performed by treatment with formaldehyde. This technology is well established and proved to be a reliable tool for detoxification of proteins for nearly a century [27]. Formaldehyde-induced inactivation approach has been successfully employed in licensed tetanus, pertussis, and diphtheria toxoid-containing vaccines (http://www.fda.gov/BiologicsBloodVaccines/Vaccines/ApprovedProducts/ucm093830.htm). Nevertheless, significant progress in the understanding of toxins' structure-function relationship as well as clarification of the fine mechanisms of toxins' actions on mammalian cells has allowed employment of site-directed mutagenesis inactivation strategies. When applicable, genetic inactivation of toxins offers an obvious advantage over chemical inactivation. First of all, site directed mutagenesis utilizes targeted replacement of amino acid residues essential for toxins' activity as opposed to indiscriminate formaldehyde-induced modifications that would ensure toxin inactivation but also could likely alter multiple epitopes potentially important for eliciting of functional (neutralizing) antibodies. These considerations influenced our initial strategy in choosing site directed mutagenesis method for detoxification of *C. difficile* toxins A and B. Introduction of amino acid substitutions in toxin A and B effectively eliminated glucosyltransferase, proteolytic, and pore-forming activities [19,20]. Nevertheless, mutated toxins still exhibited detectable cytotoxicity suggesting that yet unknown activity or activities contribute to overall cytotoxicity of these molecules [19]. This prompted us to consider chemical treatment as an additional step for elimination of residual cytotoxic activity of mutated toxins. For this purpose we choose EDC/NHS-based chemistry as an alternative to more conventional formaldehyde inactivation. Being a heterobifunctional reagent with restricted specificity, EDC reacts with carboxyl groups to form an amine-reactive *O*-acylisourea intermediate. In the presence of *N*-hydroxysulfosuccinimide (Sulfo-NHS) the amine-reactive intermediate converts into more stable sulfo-NHS ester form. This stabilized intermediate effectively reacts with primary amines provided either by a quenching reagent (glycine) or by available side chains of lysine residues within the same or neighboring molecule. Therefore, EDC/NHS treatment of TM TcdA and TM TcdB results in the modification of aspartic and glutamic acids and formation of glycine adducts as well as stable intra- and

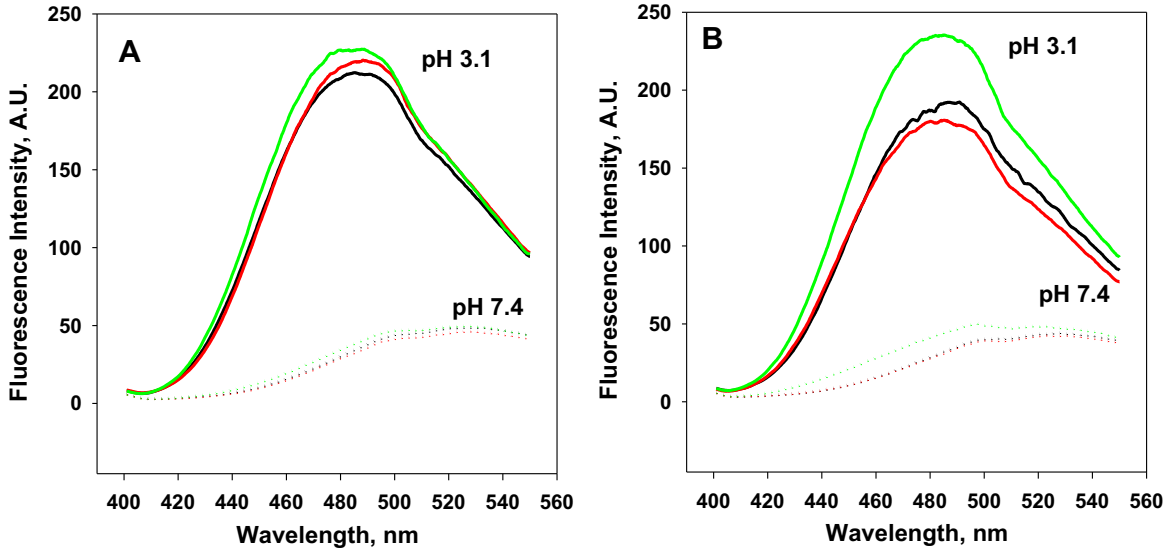

Fig. 8. ANS fluorescence emission spectra in the presence of toxins/toxoids A (panel A) and B (panel B) at neutral vs. acidic pH. Panel A: dotted lines – pH 7.4, solid lines – pH 3.1, black – TcdA, red – TM TcdA, green – TxdA. Panel B: dotted lines – pH 7.4, solid lines – pH 3.1, black – TcdB, red – TM TcdB, green – TxdB.

inter-molecular amide bonds. In addition, less common type of modifications, beta-alanine adducts, were identified in both TxdA and TxdB [21]. It is important to note that EDC/NHS-inactivated toxoids mostly retain their epitopes as was evident from the results of surface plasmon resonance (SPR) binding experiments performed with the panel of monoclonal antibodies (mAbs) [21].

In this study we applied several biophysical techniques including CD, fluorescence spectroscopy, AUC, and DSC to evaluate the effect of site directed mutagenesis and subsequent EDC/NHS treatment on the structural/hydrodynamic characteristics of toxoids A and B. The results of comparative characterization reveal overall similarity between all forms of the A and B toxoids and their parent toxins. Far UV CD, near UV CD, and intrinsic fluorescence data (Figs. 2–4) suggest that secondary and tertiary structures of TxdA and TxdB are either identical or very similar to that of their respective wild type toxins and genetically mutated parent molecules. The results of analytical ultracentrifugation experiments also showed that all three forms of toxin/toxoid A and B have very similar hydrodynamic characteristics (Fig. 5 and Table 1). Each of these proteins is an elongated and mostly monomeric molecule. Both TxdA and TxdB samples also contain a somewhat higher fraction of high molecular weight species (oligomers). This observation is consistent with the results of analytical size-exclusion chromatography experiments [21] and further illustrates the heterobifunctional nature of EDC reagent and its ability to produce intermolecular bonds.

The predominantly monomeric status of toxoids demonstrated by the results of analytical ultracentrifugation experiments indicates that the majority of low mobility TxdA and TxdB bands observed upon SDS-PAGE analysis (Fig. 1A and B, lanes 3, 6) do not represent oligomers. Most likely these bands are various TxdA and TxdB-modified species that exhibit a different (reduced) capacity to bind SDS and abnormally slow migration during electrophoresis. Therefore, even though reduced electrophoretic mobility of TxdA and TxdB samples reflects the effect of EDC/NHS-induced modifications on the proteins, it is apparent that by itself it cannot serve as an evidence of oligomerization.

Preservation of native-like conformational plasticity of TxdA and TxdB was evident from the results of ANS binding experiments. Upon shifting pH from neutral to acidic (which mimics acidic environment in early endosome) all forms of toxin/toxoid A and B undergo similar conformational rearrangements accompanied by an increase of ANS fluorescence (Fig. 8). Once again, these data indicate that neither amino acid substitutions nor EDC/NHS treatment of TxdA and TxdB alter the capacity of these molecules to properly respond to acidification of pH. The data also strongly suggest that EDC/NHS-induced crosslinks within TxdA and TxdB do not restrict mobility of the structural elements (possibly domains) participating in conformational rearrangements triggered by acidic pH.

The results of thermal unfolding experiments reveal noticeable differences between toxoids and their parent molecules. Introduction of D285A/D287A/C700A mutations in toxin A and D286A/D288A/C698A substitutions in toxin B resulted in destabilization of their respective glucosyltransferase and/or protease domain(s). It should be noted that the TM TcdB, containing two additional E970K/E976K mutations in translocation domain [19], exhibited even more pronounced destabilization of the protein resulting in the appearance of a well-defined low temperature transition that was not observed in TM TcdB mutant (data not shown). Interestingly, EDC/NHS-induced inactivation of TM TcdA resulted only in a minimal (1 °C) increase of its apparent thermostability, while the effect of EDC/NHS treatment on apparent thermostability of TM TcdB was not noticeable at all (Table 2). The most prominent change in TxdB thermogram (Fig. 7B) was increased cooperativity of unfolding, which suggests that at least some crosslink(s) introduced by EDC/NHS are likely to have inter-domain location. It could be expected that these interdomain crosslinks reduce plasticity of the molecule, which clearly was not observed in ANS binding experiments (Fig. 8B). These apparently contradicting observations could be reconciled by taking into consideration the complex multidomain organization of *C. difficile* toxins [14]. It is likely that domains contributing to increased cooperativity of TxdB thermal unfolding (crosslinked domains) and domains involved in pH induced rearrangements represent different parts of the molecule. Alternatively, it is entirely possible that ANS detected conformational changes of *C. difficile* toxins are not accompanied by major domain rearrangements but represent rather minor intradomain changes leading to the exposure of hydrophobic residues required for insertion into the lipid membrane. Either way, EDC/NHS modification did not have an impact on the ability of TxdA and TxdB to undergo conformational changes in response to acidification of pH.

Apparent thermostability data observed for TxdA and TxdB (Table 2) are considerably different from the reported results on the effect of formaldehyde on the thermal stability of *C. difficile* toxins A and B [28]. According to Salnikova et al. both formaldehyde inactivated toxoids A and B displayed about 10 °C higher apparent T*m* than their corresponding wild type (non-treated) toxins [28]. Thermal stabilization effect induced by either formaldehyde or EDC/NHS can be readily explained by the ability of these reagents to produce intramolecular covalent bonds within modified proteins. Such intramolecular crosslinks would restrict mobility of the unfolded polypeptide chain, decreasing entropy of the unfolded state, with the corresponding increase in protein stability. The degree of thermal stabilization in this case correlates with the level of modifications leading to the formation of intramolecular crosslinks. This interpretation is consistent with the rather restricted crosslinking specificity of EDC/NHS reagent and broad specificity of formaldehyde. Indeed, EDC/NHS induces the formation of crosslinks between carboxyl groups of aspartic or glutamic acids and amino groups of lysines [21,29]. In contrast, crosslinks produced by formaldehyde occur between lysine residues and susceptible side chains of arginine, glutamine, histidine, tryptophan, and tyrosine [30]. It is apparent that such a broad range of amino acid residues targeted by formaldehyde should also result in a higher degree of intermolecular crosslinking. Not surprisingly, the presence of high-molecular weight aggregates was reported for formaldehyde-inactivated toxins A and B [28]. The high degree of modifications including intra- and intermolecular crosslinking induced by formaldehyde makes this reagent extremely effective for detoxification of proteins. Unfortunately, the very same features compromise the retention of immunogenicity and / or antigenicity of formaldehyde-inactivated proteins [31,32].

In summary, detailed biophysical characterization of toxoids A and B demonstrated their structural integrity and similarity to the functionally active wild type toxins A and B. The results revealed that our “hybrid” inactivation strategy composed of sequential mutagenesis and EDC/NHS treatment of *C. difficile* toxins A and B offers a novel, gentle but very effective approach for the preparation of toxoids maintaining native-like structure and conformation.

Disclosure

This study was sponsored by Pfizer.

Acknowledgements

We would like to thank J. Moran, J. Lotvin, and P. Fink (all Pfizer) for production of mutated toxins and EDC/NHS inactivated toxoids A and B, M. Carriere (Pfizer) for assistance with protein sequence analysis. We also thank G. Zlotnick and A. S. Anderson (all Pfizer) for critical reading of the manuscript.

Appendix A. Transparency document

Transparency document associated with this article can be found in the online version at http://dx.doi.org/10.1016/j.bbrep.2016.12.015.

References

[1] C.P. Kelly, T. LaMont, *Clostridium difficile* – more difficult than ever, N. Eng. J. Med. 359 (2008) 1932–1940.

[2] J.G. Bartlett, N. Moon, T.W. Chang, N. Taylor, A.B. Onderdonk, Role of *Clostridium difficile* in antibiotic-associated pseudomembranous colitis, Gastroenterology 75 (1978) 778–782.

[3] T. Jank, K. Aktories, Structure and mode of action of clostridial glucosylating toxins: the ABCD model, Trends Microbiol. 16 (2008) 222–229.

[4] H.L. DuPont, The search for effective treatment of *Clostridium difficile* infection, N. Eng. J. Med. 364 (2011) 473–475.

[5] A.A. Venugopal, S. Johnson, Current state of *Clostridium difficile* treatment options, Clin. Infect. Dis. 55 (2012) S71–S76.

[6] G. Hussack, J. Tanha, Toxin-specific antibodies for the treatment of *Clostridium difficile*: current status and future perspectives, Toxins 2 (2010) 998–1018.

[7] L. Kyne, M. Warny, A. Qamar, C.P. Kelly, Association between antibody response to toxin A and protection against recurrent *Clostridium difficile* diarrhea, Lancet 357 (2001) 189–193.

[8] B. Aronsson, M. Granstrom, R. Mollby, C.E. Nord, Serum antibody response to *Clostridium difficile* toxins in patients with *Clostridium difficile* diarrhea, Infection 13 (1985) 97–101.

[9] D.S. Fernie, R.O. Thomson, I. Batty, P.D. Walker, Active and passive immunization to protect against antibiotic associated caecitis in hamsters, Dev. Biol. Stand. 53 (1983) 325–332.

[10] P.-H. Kim, J.P. Iaconis, R.D. Rolfe, Immunization of adult hamsters against *Clostridium difficile*- associated ileocecitis and transfer of protection to infant hamsters, Infect. Immun. 55 (1987) 2984–2992.

[11] J.F. Torres, D.M. Lyerly, J.E. Hill, T.S. Monath, Evaluation of formalin-inactivated *Clostridium difficile* vaccines administered by parenteral and mucosal routes of immunization in hamsters, Infect. Immun. 63 (1995) 4619–4627.

[12] S. Aboudola, K.L. Kotloff, L. Kyne, M. Warny, E.C. Kelly, S. Sougioultzis, P.J. Giannasca, T.P. Monath, C.P. Kelly, *Clostridium difficile* vaccine and serum immunoglobulin G antibody response to toxin A, Infect. Immun. 71 (2003) 1608–1610.

[13] F. Rebeaud, M.F. Bachmann, Immunization strategies for *Clostridium difficile* infections, Expert Rev. Vaccin. 11 (2012) 469–479.

[14] R.N. Pruitt, D.B. Lacy, Toward a structural understanding of *Clostridium difficile* toxins A and B, Front. Cell. Infect. Microbiol. 2 (2012) 1–14.

[15] C. Busch, F. Hofmann, J. Selzer, S. Munro, D. Jeckel, K. Aktories, A common motif of eukaryotic glycosyltransferases is essential for the enzyme activity of large clostridial Cytotoxins, J. Biol. Chem. 273 (1998) 19566–19572.

[16] M. Egerer, T. Giesemann, T. Jank, K.J. Fullner Satchell, K. Aktories, Auto-catalytic cleavage of *Clostridium difficile* toxins A and B depends on cysteine protease activity, J. Biol. Chem. 282 (2007) 25314–25321.

[17] L.A. Barroso, J.S. Moncrief, D.M. Lyerly, T.D. Wilkins, Mutagenesis of *Clostridium difficile* toxin B gene and effect on cytotoxic activity, Microb. Pathog. 16 (1994) 297–303.

[18] J.G.S. Ho, A. Greco, M. Rupnik, K.K.-S. Ng, Crystal structure of receptor-binding C-terminal repeats from *Clostridium difficile* toxin A, Proc. Natl. Acad. Sci. U.S.A. 102 (2005) 18373–18378.

[19] R.G.K. Donald, M. Flint, N. Kalyan, E. Johnson, S.E. Witko, C. Kotash, P. Zhao, S. Megati, I. Yurgelonis, P.K. Lee, Y.V. Matsuka, E. Severina, A. Deatly, M. Sidhu, K.U. Jansen, N.P. Minton, A.S. Anderson, A novel approach to generate a recombinant toxoid vaccine against *Clostridium difficile*, Microbiology 159 (2013) 1254–1266.

[20] S. Genisyuerek, P. Papatheodorou, G. Guttenberg, R. Schubert, R. Benz, K. Aktories, Structural determinants for membrane insertion, pore formation and translocation of *Clostridium difficile* toxin B, Mol. Microbiol. 79 (2011) 1643–1654.

[21] E. Vidunas, A. Mathews, M. Weaver, P. Cai, E.H. Koh, S. Patel-Brown, H. Yuan, Z. Zheng, M. Carriere, J.E. Johnson, J. Lotvin, J. Moran, Production and characterization of chemically inactivated genetically engineered *Clostridium difficile* toxoids, J. Pharm. Sci. 105 (2016) 2032–2041.

[22] A.F. Winder, W.L. Gent, Correction of light-scattering errors in spectrophotometric protein determinations, Biopolymers 10 (1971) 1243–1251.

[23] P. Schuck, Size-distribution analysis of macromolecules by sedimentation velocity ultracentrifugation and Lamm equation modeling, Biophys. J. 78 (2000) 1606–1619.

[24] J.R. Lakowicz, Principles of Fluorescence Spectroscopy, second ed., Kluwer Academic / Plenum Publishers, New York, 1999.

[25] L.E. Lancaster, K. Markey, M.M. Ho, An assessment of thermal stability of *Clostridium difficile* toxoid formulations, Hum. Vaccin. 7 (2011) 202–210.

[26] M. Qa'Dan, L.M. Spyres, J.D. Ballard, pH-induced conformational changes in *Clostridium difficile* toxin B, Infect. Immun. 68 (2000) 2470–2474.

[27] G. Ramon, Sur la toxine et sur l'anatoxine diphtheriques, Ann. Inst. Pasteur 38 (1924) 1–18.

[28] M. Salnikova, S.B. Joshi, J.H. Rytting, M. Warny, C.R. Middaugh, Physical characterization of *Clostridium difficile* toxins and toxoids: effect of the formaldehyde crosslinking on thermal stability, J. Pharm. Sci. 97 (2008) 3735–3752.

[29] R.L. Lundblad, The Modification of Carboxyl Groups, In: Techniques in Protein Modification, CRC Press, Boca Raton, 1995, pp. 233–247.

[30] B. Metz, G.F.A. Kersten, A. de Jong, H. Meiring, J. ten Hove, W.E. Hennink, D.J.A. Crommelin, W. Jiskoot, Identification of formaldehyde-induced modifications in proteins: reactions with diphtheria toxin, in: B. Metz (Ed.)Structural Characterization of Diphtheria Toxoid, Print Partners Ipskamp B.V. Enschede, 2005, pp. 141–154.

[31] L. Nencioni, G. Volpini, S. Peppoloni, M. Bugnoli, T. De Magistris, I. Marsili, R. Rappuoli, Properties of pertussis toxin mutant PT-9K/129G after formaldehyde treatment, Infect. Immun. 59 (1991) 625–630.

[32] A. Di Tommaso, M.T. De Magistris, M. Bugnoli, I. Marsili, R. Rappuoli, S. Abrignani, Formaldehyde treatment of proteins can constrain presentation to T cells by limiting antigen processing, Infect. Immun. 62 (1994) 1830–1834.